Supplemental Material

The working stroke of the myosin II motor in muscle is not tightly coupled to release of orthophosphate from its active site.

Marco Caremani, Luca Melli, Mario Dolfi, Vincenzo Lombardi and Marco Linari

Laboratory of Physiology, Department of Biology, University of Florence
Sesto Fiorentino, 50019, Italy

1. Model computation

The model combines the kinetic scheme able to simulate the effects of changes in [Pi] on the force and ATPase rate of the isometric contraction (Linari *et al.*, 2010) and the Huxley and Simmons model of the working stroke (Huxley & Simmons, 1971), which implies different conformations of the attached motors (black transitions in Figure 4*A*). In addition the model implies the possibility for individual myosin motors to slip between two consecutive actin monomers while they are at an intermediate stage of their biochemical and structural cycle (red transitions in Figure 4*A*).

M.ATP, M.ADP.Pi-AM.ADP.Pi, M*.ADP.Pi are detached states, AM_i.ADP.Pi, AM_i.ADP and AM_i are states attached to an actin monomer (A) and A'M_i.ADP.Pi, A'M_i.ADP and A'M_i are states attached to the next actin monomer (A') on the same strand shifted by 5.5 nm farther from the centre of the sarcomere, with i varying from 1 to m according to the number of structural states assumed during the working stroke. The structural change underlying the working stroke is represented by (m-1) stepwise transitions each responsible for an axial movement z (Brunello *et al.*, 2007). As detailed in previous work (Piazzesi & Lombardi, 1995; Woledge *et al.*, 2009; Park-Holohan *et al.*, 2012), the value of z is constrained by the stiffness of the myosin motor. Under the conditions of this work the average motor stiffness ε is 1.2 pN nm^{-1} (see (Linari *et al.*, 2007)) and z is chosen 3.1 nm. Substantially similar results are obtained in a simulation where ε is taken = 1.7 pN nm^{-1}, according to the estimate obtained when the lattice dimension of the intact fibre is recovered by osmotic compression (Linari *et al.*, 2007). Three steps of 3.1 nm are necessary to fit both the kinetic requirements necessary to simulate force and velocity transients following length and force steps respectively (Piazzesi *et al.*, 2002; Woledge *et al.*, 2009; Park-Holohan *et al.*, 2012) and the mechanical and structural constraints of a maximum working stroke of ~10 nm (Huxley & Simmons, 1971; Rayment *et al.*, 1993). Thus there are four structural states of the attached motor (M_1, M_2, M_3 and M_4) and three transitions ($M_1 \rightarrow M_2$, $M_2 \rightarrow M_3$, $M_3 \rightarrow M_4$).

The following assumptions integrate those reported in Piazzesi and Lombardi model (Piazzesi & Lombardi, 1995). A myosin head can attach in the AM_1.ADP.Pi state to one actin site (A) for a range of positions λ = 5.5 nm, from x = -2.75 to 2.75 nm (where x is the relative axial position between the myosin head and A, and is zero for the centre of distribution of attachments of the motors in the M_1 state). ξ is the value x assumes within λ ($-2.75 \leq \xi \leq 2.75$). Myosin heads are uniformly distributed along x so that, in isometric conditions, for each value of ξ the sum of all attached and detached heads is 1. The periodic boundary conditions are the same as those used in (Piazzesi & Lombardi, 1995) implying that (*i*) in isometric conditions at the two

extremities of λ there are no attached myosin heads and the sum of detached states is 1; (*ii*) sliding in the shortening direction shifts the distribution of the attached heads to negative x values beyond λ. When a myosin head detaches, the time for the head to regain the original configuration is assumed to be very short (tens of microseconds). Provided that the rate of reverse reaction at the site of detachment is low with respect to the resetting time of the myosin head, all the heads detaching at a given x beyond λ regain the position, within λ, given by $\xi = x - p\lambda$, where p (negative for shortening and positive for lengthening) is the number of times the attached head has exceeded one boundary in the same direction. During sliding the sum of the fractional occupancies of all states $N(\xi) = 1$ is given by the equation:

$$N(\xi) = MATP(\xi) + MADPPi(\xi) + M^{*}ADPPi(\xi) + \sum_{i=1}^{4} AM_{i}ADPPi(\xi + p\lambda) + \sum_{i=1}^{4} AM_{i}ADP(\xi + p\lambda) +$$
$$\sum_{i=1}^{4} AM_{i}(\xi + p\lambda) + \sum_{i=1}^{4} A'M_{i}ADPPi(\xi + p\lambda) + \sum_{i=1}^{4} A'M_{i}ADP(\xi + p\lambda) + \sum_{i=1}^{4} A'M_{i}(\xi + p\lambda) = 1$$

For any steady state mechanical condition (isometric contraction or steady shortening), the total flux of energy can be calculated from the flux between the states M.ATP and M.ADP.Pi-AM.ADP.Pi (step 2) or M.ADP.Pi-AM.ADP.Pi and AM_1.ADP.Pi (step 3) in the cycle (Figure 4*A*). The free energy of hydrolysis of one molecule of MgATP (ΔG^{ATP}) can be expressed as:

$$\Delta G^{ATP} = \Delta G_0 + k_B \Theta \ln \frac{[ATP]}{[ADP][Pi]}$$

where k_B (=1.381*10^{-23} J K^{-1}) is the Boltzmann constant, Θ (=285.15 K) is the absolute temperature and ΔG_0 is the standard free energy. ΔG^{ATP} is assumed to be 100 zJ in the control condition (MgATP, 5 mM; free ADP, 30 μM and free Pi, 1 mM) ((Barclay *et al.*, 2010) and references therein) and it reduces by rising [Pi]: addition of 10 mM Pi will lower the free energy by about 10 zJ (see Figure S1).

The equations expressing the x-dependence of the reaction rates are reported in Table S1. The distribution of myosin heads at any given time is calculated by numerical integration of the differential equations reported in Table S2.

The free energy profile ($G(x)$, Figures 4*C* and S1) of the various states are related to the forward $k_i(x)$ and reverse $k_{-i}(x)$ rate constants of the transition between neighbouring states k and l through the Gibbs equation:

$$k_i(x) / k_{-i}(x) = \exp[(G_k(x) - G_l(x)) / k_B \Theta]$$

One rate constant of the pair is calculated from the above equation after choosing the appropriate value for the other.

The free energy profiles of the attached states are parabolic according to the assumption that the motor stiffness ε, the second order derivative of the energy, is constant. Two consecutive structural states of the motor attached to actin A in the same biochemical state have the free energy parabolas shifted on x by the step size (3.1 nm) and the difference in their free energy minima is 12 zJ independently of the biochemical state. Thus the total energy change associated to the three structural transitions ($M_1 \rightarrow M_2$, $M_2 \rightarrow M_3$ and $M_3 \rightarrow M_4$) while the motor is attached to the same actin monomer A is 36 zJ (Figure 4*C*).

The biochemical step in the attached states, consists in a downward shift of the free energy parabolas for each given structural state: the drop in the free energy minimum induced by Pi release is 15.4 zJ in control solution (no added Pi) and 6 zJ in 10 mM Pi; the difference in free energy minimum induced by release of ADP in 5.1 zJ. The diagrams of the free energy profiles for the different biochemical states of the same structural state (M_1, continuous lines and M_4, dashed lines) without (black) and with 10 mm added Pi (green), are shown in Figure S1.

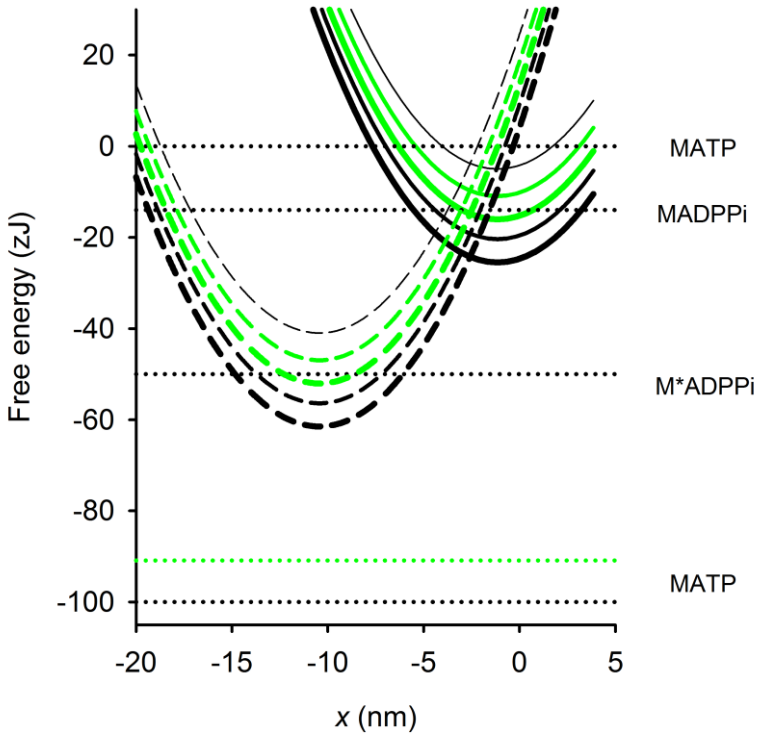

Figure S1. Free energy diagrams of the myosin motor attached to the actin monomer A in the different biochemical states (from the thinnest to the thickest line, AM.ADP.Pi, AM.ADP and AM). Only two of the four structural states are shown for clarity, M_1 (continuous lines) and M_4 (dashed lines). The black lines are in the control solution (no added Pi) and the horizontal lines show the free energy of the detached states. The green lines show the effect of the addition of 10 mM Pi on the free energy level of the AM.ADP, AM and M.ATP states (the upward shift accounting for the reduction in ΔG).

Slipping of M_2 and M_3 motors in either AM.ADP.Pi or AM.ADP state from the original actin monomer (A) to the next actin monomer (A') is controlled by a transition possible in a narrow range of x values where the strain of the A-attached motor is near zero and the motor dwells between two possibilities, either to progress to the next structural state on the same actin, or to slip *to* A' and then undergo the state re-equilibration promoted by the 5.5 nm increase in strain (Figures 4*B* and *C*).

In isometric conditions the time step for integration (Δt) was 25 μs. The simulation started with myosin heads distributed between M.ATP and AM.ADP.Pi states according to the equilibrium constant. The fraction of myosin heads in each state was calculated with an interval (Δx) of 0.025 nm. Because detached myosin heads exist only within λ there are (5.5/0.025 =) 220 discrete positions for which the isometric distribution is calculated. The fractional occupancy of the various states at the steady state of the isometric contraction is shown as a function of x in Figure S2.

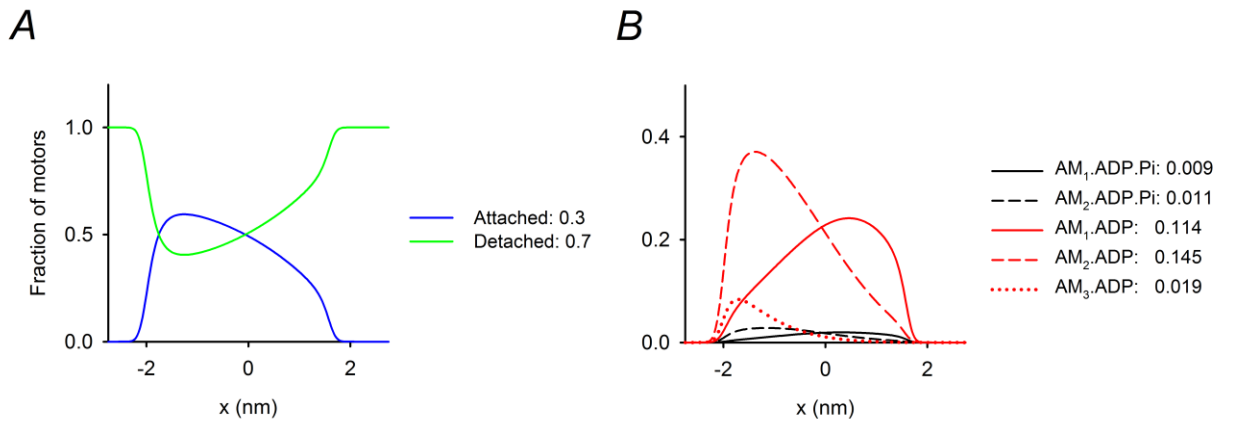

Figure S2 *A*. x distribution of the fraction of myosin motors in the detached (green) and the attached state (blue) during an isometric contraction. *B*. Fractional occupancy of the various attached states, according to the colour code and the figures in the inset. States not represented here contribute for a fraction < 0.005

The ratio of the number of myosin heads in the AM.ADP.Pi state over that in the AM.ADP state is about 0.09 with about 93% of the AM.ADP myosin motors in the M_1 and M_2 states.

During the isotonic velocity transient Δt was 25 μs, while during ramp shortening Δt was chosen according to sliding velocity.

The step perturbation in force is complete in zero time, consequently, the simulated length response at the end of the force step (phase 1) is not affected by the rapid phase 2 shortening as in the experimental records (Figure 1).

With the distribution of attached states during isometric contraction as in Figure S2*B*, the average motor strain (*s*) is 3.4 nm and thus the isometric force developed by a single myosin motor is $F = (\varepsilon \cdot s =)$ 4.1 pN. Since only 30% of all the heads are attached in the isometric contraction, corresponding to (300·0.30=) 90 myosin motors per half thick filament, the force per half-thick filament is (4.1 pN · 90=) 370 pN. With $0.41 \cdot 10^{15}$ thick filaments per cross sectional area (Brenner & Yu, 1991; Kawai *et al.*, 1993) the force of the fibre is (370 pN/thick filament · $0.41 \cdot 10^{15}$ thick filament/m^2=) 152 kPa, within the range of isometric force found in this preparation ((Linari *et al.*, 2007; Caremani *et al.*, 2008) and Table 1).

The force generated by an attached myosin motor at a given x (F_x) between x-$\Delta x/2$ and x+$\Delta x/2$ is calculated as

$$F_x = \varepsilon\left(\sum_{j=b_1}^{b_3} xAM1_{j,x} + \sum_{j=b_1}^{b_3}(x+z)AM2_{j,x} + \sum_{j=b_1}^{b_3}(x+2z)AM3_{j,x} + \sum_{j=b_1}^{b_3}(x+3z)AM4_{j,x} + \right.$$
$$\left.\sum_{j=b_1}^{b_3}(x+a)A'M1_{j,x} + \sum_{j=b_1}^{b_3}(x+a+z)A'M2_{j,x} + \sum_{j=b_1}^{b_3}(x+a+2z)A'M3_{j,x} + \sum_{j=b_1}^{b_3}(x+a+3z)A'M4_{j,x}\right)$$

Where j identifies the three biochemical states (b_1=AM.ADP.Pi, b_2=AM.ADP and b_3=AM) and a (=5.5 nm) is the increase in strain of a motor slipping from the first (A) to the second actin (A').

The average force (F) generated by the population of the attached myosin heads is calculated by integrating F_x over x.

2. Kinetic requirements during shortening.

For the model to fit the isotonic velocity transient and the steady power, it is assumed that attached motors engaged in the working stroke in either the AM.ADP.Pi state or AM.ADP state can slip to the next actin monomer farther from the centre of the sarcomere, while the actin filament is sliding along for the collective action of the other motors on the same filament.

Figure S3 shows how the fluxes through the conventional path (blue line, steps 4, 5 and 1 of the scheme in Figure 4*A*), the early detachment path (green line, steps 6 and 7) and the slip to the second actin (red line, either step 8 or 9 followed by the termination of the working stroke on A') contribute to the total ATPase rate (black line) at each shortening velocity. The flux of the myosin motors slipping to the second actin, is zero in isometric contraction, when 0.75 of the total ATPase rate is due to the flux through the conventional path and 0.25 to the flux trough the early detachment path (ordinate intercepts in Figure S3). The flux of motors using two actins (red) rises sharply with the shortening velocity and in the region of $V < 1000$ nm s^{-1}, corresponding to that for the maximum power, attains a value that is 0.4 the total ATPase rate, a fraction comparable to that provided by motors cycling through the conventional path (blue). At $V \geq 1000$ nm s^{-1} the flux of slipping motors decreases with the increase in shortening speed and, at V_0, becomes ~0.1 the total ATPase rate, while ~0.7 is contributed by the flux through the conventional cycle and ~0.2 by the flux through the early detachment.

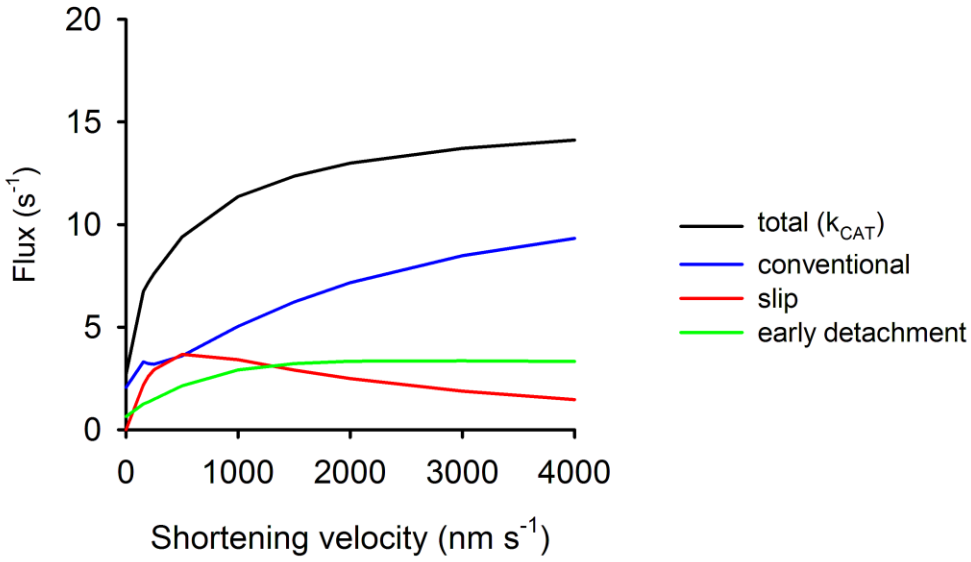

Figure S3. Dependence on shortening velocity of the total flux of myosin motors contributing to the ATPase rate (black line) and of its fractions: blue line, flux of myosin motors that complete the cycle on the same actin monomer A (conventional); red line, flux of myosin motors slipping to the second actin (A') to complete the cycle (slip); green line, flux of myosin motors that detach with both ligands (early detachment).

Table S1 Equations expressing the x-dependence of the rate constants of the forward transitions in the reaction scheme according to the direction of the reaction flow during steady shortening. The rate constants of the transitions between different biochemical states or between different actin monomers are indicated as k_{lm} where l (from 1 to 9) identifies the transition according to the scheme of Figure 4*A* and m ($M_1 \rightarrow M_4$) indicates the structural state involved in the transition. The rate constant of the structural transitions for the same biochemical state are indicated as k_w with w = w1, w2 and w3 for the transitions $M_1 \rightarrow M_2$, $M_2 \rightarrow M_3$ and $M_3 \rightarrow M_4$ respectively. These "structural" rate constants have the same x-dependence for the different biochemical states but their values are multiplied by 0.01 for AM and A'M states. x_0 is the strain of the M_1 state at x=0, which has been set to 1.15 nm. (') is added to the subscript if the transition occurs on the second actin.

$k_{1,\,M1}$ ($M^{-1}\,s^{-1}$)	$= 10^5$	
$k_{1,\,M2}$ ($M^{-1}\,s^{-1}$)	$= 10^5$	
$k_{1,\,M3}$ ($M^{-1}\,s^{-1}$)	$= 10^5$	
$k_{1,\,M4}$ ($M^{-1}\,s^{-1}$)	$= 4.16 \cdot 10^5$ $= -1.92 \cdot 10^5 \cdot (x+x_0+7.48)$ $= 10^5$	$x < -10.75$ $-10.75 \le x < -9.15$ $x \ge -9.15$
$k_{1',\,M1}$ ($M^{-1}\,s^{-1}$)	$= 10^5$	
$k_{1',\,M2}$ ($M^{-1}\,s^{-1}$)	$= 10^5$	
$k_{1',\,M3}$ ($M^{-1}\,s^{-1}$)	$= 10^5$	
$k_{1',\,M4}$ ($M^{-1}\,s^{-1}$)	$= 4 \cdot 10^5$ $= -1.85 \cdot 10^5 \cdot (x+x_0+7.48)$ $= 10^5$	$x < -16.25$ $-16.25 \le x < -14.65$ $x \ge -14.65$
k_2 (s^{-1})	$= 30$	
k_3 (s^{-1})	$= 70 \cdot \exp \cdot (-0.1 \cdot (x+x_0-1.5)^6)$	
$k_{4,\,M1}$ (s^{-1}), $k_{4',\,M1}$ (s^{-1})	$= 60$	
$k_{4,\,M2}$ (s^{-1}), $k_{4',\,M2}$ (s^{-1})	$= 100$	
$k_{4,\,M3}$ (s^{-1}), $k_{4',\,M3}$ (s^{-1})	$= 1000$	
$k_{4,\,M4}$ (s^{-1}), $k_{4',\,M4}$ (s^{-1})	$= 5000$	
$k_{5,\,M1}$ (s^{-1})	$= 1.62$ $= -0.2 \cdot (x+ x_0+0.9)$ $= 0.02$	$x < -10.15$ $-10.15 \le x < -2.15$ $x \ge -2.15$
$k_{5,\,M2}$ (s^{-1})	$= 171$ $= -20 \cdot (x+ x_0-3)$ $= -180 \cdot (x+ x_0+0.73)$ $= 12$	$x < -6.65$ $-6.65 \le x < -2.35$ $-2.35 \le x < -1.95$ $x \ge -1.95$
$k_{5,\,M3}$ (s^{-1})	$= 225$ $= -40 \cdot (x+ x_0-4.9)$ $= -20 \cdot (x+ x_0+3.6)$ $= 18$	$x < -11.65$ $-11.65 \le x < -7.35$ $-7.35 \le x < -5.65$ $x \ge -5.65$
$k_{5,\,M4}$ (s^{-1})	$= 9808$ $= -1500 \cdot (x+ x_0+1.85)$ $= -200 \cdot (x+ x_0+8.46)$ $= -60 \cdot (x+ x_0+6.5)$ $= 30$	$x < -26.15$ $-26.15 \le x < -21.15$ $-21.15 \le x < -10.45$ $-10.45 \le x < -8.15$ $x \ge -8.15$
$k_{5',\,M1}$ (s^{-1})	$= 15.2$ $= -4 \cdot (x+ x_0+6.45)$ $= -(x+ x_0+4.8)$ $= 0.2$	$x < -11.15$ $-11.15 \le x < -8.15$ $-8.15 \le x < -6.15$ $x \ge -6.15$
$k_{5',\,M2}$ (s^{-1})	$= 133.8$ $= -20 \cdot (x+ x_0+7.86)$ $= -3 \cdot (x+ x_0+3.6)$	$x < -15.65$ $-15.65 \le x < -9.75$ $-9.75 \le x < -8.15$

	$= 10$	$x \geq -8.15$
$k_{5', M3}$ (s^{-1})	$= 222$ $= -40 \cdot (x + x_0 + 10.47)$ $= -20 \cdot (x + x_0 + 9.25)$ $= 15$	$x < -17.15$ $-17.15 \leq x < -12.85$ $-12.85 \leq x < -11.15$ $x \geq -11.15$
$k_{5', M4}$ (s^{-1})	$= 1469$ $= -1500 \cdot (x + x_0 + 23.96)$ $= -200 \cdot (x + x_0 + 13.96)$ $= -60 \cdot (x + x_0 + 12)$ $= 30$	$x < -31.65$ $-31.65 \leq x < -26.65$ $-26.65 \leq x < -15.95$ $-15.95 \leq x < -13.65$ $x \geq -13.65$
$k_{6, M1}$ (s^{-1})	$= 82$ $= -10 \cdot (x + x_0 - 7)$ $= 70$	$x < -2.35$ $-2.35 \leq x < -1.15$ $x \geq -1.15$
$k_{6, M2}$ (s^{-1})	$= 1860$ $= -600 \cdot (x + x_0 + 0.4)$ $= 0$	$x < -4.65$ $-4.65 \leq x < -1.55$ $x \geq -1.55$
$k_{6, M3}$ (s^{-1})	$= 990$ $= -300 \cdot (x + x_0 + 3.5)$ $= 0$	$x < -7.95$ $-7.95 \leq x < -4.65$ $x \geq -4.65$
$k_{6, M4}$ (s^{-1})	$= 950$ $= -500 \cdot (x + x_0 + 9.3)$ $= 0$	$x < -12.35$ $-12.35 \leq x < -10.45$ $x \geq -10.45$
k_7 (s^{-1})	$= 500$	
$k_{8, M2}$ (s^{-1})	$= 100 \cdot \exp(-z\varepsilon(x + x_0 + 0.5 + z)/k_B\theta)/(1 + \exp(-z\varepsilon(x + x_0 + 0.5)/k_B\theta)$ $= 0$	$x < -1$ $x \geq -1$
$k_{8, M3}$ (s^{-1})	$= 40 \cdot \exp(-z\varepsilon(x + x_0 + 1.5 + 2z)/k_B\theta)/(1 + \exp(-z\varepsilon(x + x_0 + 0.5)/k_B\theta)$ $= 0$	$x < -1$ $x \geq -1$
$k_{9, M2}$ (s^{-1})	$= 380 \cdot \exp(-z\varepsilon(x + x_0 + 0.5 + z)/k_B\theta)/(1 + \exp(-z\varepsilon(x + x_0 + 0.5)/k_B\theta)$ $= 0$	$x < -1$ $x \geq -1$
$k_{9, M3}$ (s^{-1})	$= 900 \cdot \exp(-z\varepsilon(x + x_0 + 1.5 + 2z)/k_B\theta)/(1 + \exp(-z\varepsilon(x + x_0 + 1.5)/k_B\theta)$ $= 0$	$x < -1$ $x \geq -1$
k_{w1} (s^{-1})	$= 52500 \cdot \exp(-z\varepsilon(x + x_0 - 0.5)/k_B\theta)/(1 + \exp(-z\varepsilon(x + x_0 - 0.5)/k_B\theta)$	
k_{w2} (s^{-1})	$= 24500 \cdot \exp(-z\varepsilon(x + x_0 - 0.5 + z)/k_B\theta)/(1 + \exp(-z\varepsilon(x + x_0 - 0.5 + z)/k_B\theta)$	
k_{w3} (s^{-1})	$= 14000 \cdot \exp(-z\varepsilon(x + x_0 - 0.5 + 2z)/k_B\theta)/(1 + \exp(-z\varepsilon(x + x_0 - 0.5 + 2z)/k_B\theta)$	
$k_{w1'}$ (s^{-1})	$= 52500 \cdot \exp(-z\varepsilon(x + x_0 + 5)/k_B\theta)/(1 +$	

	$\exp(-z\varepsilon(x+x_0+5)/k_B\theta)$	
$k_{w2'}$ (s^{-1})	$= 24500\cdot\exp(-z\varepsilon(x+x_0+5+z)/k_B\theta)/(1+\exp(-z\varepsilon(x+x_0+5+z)/k_B\theta)$	
$k_{w3'}$ (s^{-1})	$= 14000\cdot\exp(-z\varepsilon(x+x_0+5+2z)/k_B\theta)/(1+\exp(-z\varepsilon(x+x_0+5+2z)/k_B\theta)$	

Table S2 Differential equations used to calculate the rates of the transition between consecutive states

$\delta MATP(x, t)/\delta t = k_{-2}(x)AMADPPi(x, t) + k_{1,M1}(x)AM_1(x, t) + k_{1,M2}(x)AM_2(x, t) + k_{1,M3}(x)AM_3(x, t) + k_{1,M4}(x)AM_4(x, t) + k_{1',M1}(x)A'M_1(x, t) + k_{1',M2}(x)A'M_2(x, t) + k_{1',M3}(x)A'M_3(x, t) + k_{1',M4}(x)A'M_4(x, t) + k_7(x)M^*ADPPi(x, t) - (k_2(x) + k_{-1,M1}(x) + k_{-1,M2}(x) + k_{-1,M3}(x) + k_{-1,M4}(x) + k_{-1',M1}(x) + k_{-1',M2}(x) + k_{-1',M3}(x) + k_{-1',M4}(x) + k_{-7}(x)) \cdot MATP(x, t) - v(\delta MATP(x, t)/\delta x);$

$\delta AMADPPi(x, t)/\delta t = k_2(x)MATP(x, t) + k_{-3}(x)AM_1ADPPi(x, t) - (k_{-2}(x) + k_3(x)) \cdot AMADPPi(x, t) - v(\delta AMADPPi(x, t)/\delta x);$

$\delta AM_1ADPPi(x, t)/\delta t = k_3(x)AMADPPi(x, t) + k_{-4,M1}(x)AM_1ADP(x, t) + k_{-1w}(x)AM_2ADPPi(x, t) + k_{-6,M1}(x)M^*ADPPi(x, t) - (k_{-3}(x) + k_{4,M1}(x) + k_{1w}(x) + k_{6,M1}(x)) \cdot AM_1ADPPi (x, t) - v(\delta AM_1ADPPi (x, t)/\delta x);$

$\delta AM_2ADPPi(x, t)/\delta t = k_{1w}(x)AM_1ADPPi(x, t) + k_{-4,M2}(x)AM_2ADP(x, t) + k_{-2w}(x)AM_3ADPPi(x, t) + k_{-6,M2}(x)M^*ADPPi(x, t) + k_{-8,M2}(x)A'M_2ADPPi(x, t) - (k_{-1w}(x) + k_{4,M2}(x) + k_{2w}(x) + k_{8,M2}(x) + k_{6,M2}(x)) \cdot AM_2ADPPi (x, t) - v(\delta AM_2ADPPi (x, t)/\delta x);$

$\delta AM_3ADPPi(x, t)/\delta t = k_{w2}(x)AM_2ADPPi(x, t) + k_{-4,M3}(x)AM_3ADP(x, t) + k_{-w3}(x)AM_4ADPPi(x, t) + k_{-6,M3}(x)M^*ADPPi(x, t) + k_{-8,M3}(x)A'M_3ADPPi(x, t) - (k_{-w2}(x) + k_{4,M3}(x) + k_{w3}(x) + k_{6,M3}(x) + k_{8,M3}(x)) \cdot AM_3ADPPi (x, t) - v(\delta AM_3ADPPi (x, t)/\delta x);$

$\delta AM_4ADPPi(x, t)/\delta t = k_{w3}(x)AM_3ADPPi(x, t) + k_{-4,M4}(x)AM_4ADP(x, t) + k_{-6,M4}(x)M^*ADPPi(x, t) - (k_{-w3}(x) + k_{4,M4}(x) + k_{6,M4}(x)) \cdot AM_4ADPPi (x, t) - v(\delta AM_4ADPPi (x, t)/\delta x);$

$\delta AM_1ADP(x, t)/\delta t = k_{4,M1}(x)AM_1ADPPi(x, t) + k_{-5,M1}(x)AM_1(x, t) + k_{-w1}(x)AM_2ADP(x, t) - (k_{-4,M1}(x) + k_{5,M1}(x) + k_{w1}(x)) \cdot AM_1ADP(x, t) - v(\delta AM_1ADP (x, t)/\delta x);$

$\delta AM_2ADP(x, t)/\delta t = k_{w1}(x)AM_1ADP(x, t) + k_{-5,M2}(x)AM_2(x, t) + k_{-w2}(x)AM_3ADP(x, t) + k_{-9,M2}(x)A'M_2ADP(x, t) + k_{4,M2}(x)AM_2ADPPi(x, t) - (k_{-1w}(x) + k_{5,M2}(x) + k_{w2}(x) + k_{9,M2}(x) + k_{-4,M2}(x)) \cdot AM_2ADP(x, t) - v(\delta AM_2ADP (x, t)/\delta x);$

$\delta AM_3ADP(x, t)/\delta t = k_{w2}(x)AM_2ADP(x, t) + k_{-5,M3}(x)AM_3(x, t) + k_{-w3}(x)AM_4ADP(x, t) + k_{4,M3}(x) AM_3ADPPi(x, t) + k_{-9,M3}(x)A'M_3ADP(x, t) - (k_{-w2}(x) + k_{5,M3}(x) + k_{w3}(x) + k_{-4,M3}(x) + k_{9,M3}(x)) \cdot AM_3ADP(x, t) - v(\delta AM_3ADP (x, t)/\delta x);$

$\delta AM_4ADP(x, t)/\delta t = k_{w3}(x)AM_3ADP(x, t) + k_{-5,M4}(x)AM_4(x, t) + k_{4,M4}(x) AM_4ADPPi(x, t) - (k_{-w3}(x) + k_{5,M4}(x) + k_{-4,M4}(x)) \cdot AM_4ADP(x, t) - v(\delta AM_4ADP (x, t)/\delta x);$

$\delta AM_1(x, t)/\delta t = k_{5,M1}(x)AM_1ADP(x, t) + k_{-1,M1}(x)MATP(x, t) + k_{-w1}(x)AM_2(x, t) - (k_{-5,M1}(x) + k_{1,M1}(x) + k_{w1}(x)) \cdot AM_1(x, t) - v(\delta AM_1 (x, t)/\delta x);$

$\delta AM_2(x, t)/\delta t = k_{5,M2}(x)AM_2ADP(x, t) + k_{-1,M2}(x)MATP(x, t) + k_{w1}(x)AM_1(x, t) + k_{-w2}\, x)AM_3(x, t) - (k_{-5,M2}(x) + k_{1,M2}(x) + k_{-w1}(x) + k_{w2}(x)) \cdot AM_2(x, t) - v(\delta AM_2 (x, t)/\delta x);$

$\delta AM_3(x, t)/\delta t = k_{5,M3}(x)AM_3ADP(x, t) + k_{-1,M3}(x)MATP(x, t) + k_{w2}(x)AM_2(x, t) + k_{-w3}(x)AM_4(x, t) - (k_{-5,M3}(x) + k_{1,M3}(x) + k_{-w2}(x) + k_{w3}(x)) \cdot AM_3(x, t) - v(\delta AM_3 (x, t)/\delta x);$

$\delta AM_4(x, t)/\delta t = k_{5,M4}(x)AM_4ADP(x, t) + k_{-1,M4}(x)MATP(x, t) + k_{w3}(x)AM_3(x, t) - (k_{-5,M4}(x) + k_{1,M4}(x) + k_{-w3}(x)) \cdot AM_4(x, t) - v(\delta AM_4(x, t)/\delta x)$;

$\delta M^*ADPPi(x, t)/\delta t = k_{6,M1}(x)AM_1ADPPi(x, t) + k_{6,M2}(x)AM_2ADPPi(x, t) + k_{6,M3}(x)AM_3ADPPi(x, t) + k_{6,M4}(x)AM_4ADPPi(x, t) + k_{-7}(x)MATP(x, t) - (k_{-6,M1}(x) + k_{-6,M2}(x) + k_{-6,M3}(x) + k_{-6,M4}(x) + k_7(x)) \cdot M^*ADPPi(x, t) - v(\delta M^*ADPPi(x, t)/\delta x)$;

$\delta A'M_1ADPPi(x, t)/\delta t = k_{-4',M1}(x)A'M_1ADP(x, t) + k_{-w1}(x)A'M_2ADPPi(x, t) - (k_{4',M1}(x) + k_{w1}(x)) \cdot A'M_1ADPPi(x, t) - v(\delta A'M_1ADPPi(x, t)/\delta x)$;

$\delta A'M_2ADPPi(x, t)/\delta t = k_{-4',M2}(x)A'M_2ADP(x, t) + k_{w1}(x)A'M_1ADPPi(x, t) + k_{-w2}(x)A'M_3ADPPi(x, t) + k_{8,M2}(x)AM_2ADPPi(x, t) - (k_{4',M2}(x) + k_{-w1}(x) + k_{w2}(x) + k_{-8,M2}(x)) \cdot A'M_2ADPPi(x, t) - v(\delta A'M_2ADPPi(x, t)/\delta x)$;

$\delta A'M_3ADPPi(x, t)/\delta t = k_{-4',M3}(x)A'M_3ADP(x, t) + k_{w2}(x)A'M_2ADPPi(x, t) + k_{-w3}(x)A'M_4ADPPi(x, t) + k_{8,M3}(x)AM_3ADPPi(x, t) - (k_{4',M3}(x) + k_{-w2}(x) + k_{w3}(x) + k_{-8,M3}(x)) \cdot A'M_3ADPPi(x, t) - v(\delta A'M_3ADPPi(x, t)/\delta x)$;

$\delta A'M_4ADPPi(x, t)/\delta t = k_{-4',M4}(x)A'M_4ADP(x, t) + k_{w3}(x)A'M_3ADPPi(x, t) - (k_{4',M4}(x) + k_{-w3}(x)) \cdot A'M_4ADPPi(x, t) - v(\delta A'M_4ADPPi(x, t)/\delta x)$;

$\delta A'M_1ADP(x, t)/\delta t = k_{-5',M1}(x)A'M_1(x, t) + k_{-w1}(x)A'M_2ADP(x, t) + k_{4',M1}(x)A'M_1ADPPi(x, t) - (k_{5',M1}(x) + k_{1w}(x) + k_{-4',M1}(x)) \cdot A'M_1ADP(x, t) - v(\delta A'M_1ADP(x, t)/\delta x)$;

$\delta A'M_2ADP(x, t)/\delta t = k_{-5',M2}(x)A'M_2(x, t) + k_{w1}(x)A'M_1ADP(x, t) + k_{4',M2}(x)A'M_2ADPPi(x, t) + k_{-w2}(x)A'M_3ADP(x, t) + k_{9,M2}(x)AM_2ADP(x, t) - (k_{5',M2}(x) + k_{-w1}(x) + k_{-4',M2}(x) + k_{w2}(x) + k_{-9,M2}(x)) \cdot A'M_2ADP(x, t) - v(\delta A'M_2ADP(x, t)/\delta x)$;

$\delta A'M_3ADP(x, t)/\delta t = k_{-5',M3}(x)A'M_3(x, t) + k_{w2}(x)A'M_2ADP(x, t) + k_{4',M3}(x)A'M_3ADPPi(x, t) + k_{-w3}(x)A'M_4ADP(x, t) + k_{9,M3}(x)AM_3ADP(x, t) - (k_{5',M3}(x) + k_{-w2}(x) + k_{-4',M3}(x) + k_{w3}(x) + k_{-9,M3}(x)) \cdot A'M_3ADP(x, t) - v(\delta A'M_3ADP(x, t)/\delta x)$;

$\delta A'M_4ADP(x, t)/\delta t = k_{-5',M4}(x)A'M_4(x, t) + k_{w3}(x)A'M_3ADP(x, t) + k_{4',M4}(x)A'M_4ADPPi(x, t) - (k_{5',M4}(x) + k_{-w3}(x) + k_{-4',M4}(x)) \cdot A'M_4ADP(x, t) - v(\delta A'M_4ADP(x, t)/\delta x)$;

$\delta A'M_1(x, t)/\delta t = k_{5',M1}(x)\ A'M_1ADP(x, t) + k_{-1',M1}(x)MATP(x, t) + k_{-w1}(x)\ A'M_2(x, t) - (k_{-5',M1}(x) + k_{1',M1}(x) + k_{w1}(x)) \cdot A'M_1(x, t) - v(\delta A'M_1(x, t)/\delta x)$;

$\delta\ A'M_2(x, t)/\delta t = k_{5',M2}(x)\ A'M_2ADP(x, t) + k_{-1',M2}(x)MATP(x, t) + k_{w1}(x)\ A'M_1(x, t) + k_{-w2}(x)\ A'M_3(x, t) - (k_{-5',M2}(x) + k_{1',M2}(x) + k_{-w1}(x) + k_{w2}(x)) \cdot A'M_2(x, t) - v(\delta A'M_2(x, t)/\delta x)$;

$\delta\ A'M_3(x, t)/\delta t = k_{5',M3}(x)\ A'M_3ADP(x, t) + k_{-1',M3}(x)MATP(x, t) + k_{w2}(x)\ A'M_2(x, t) + k_{-w3}(x)\ A'M_4(x, t) - (k_{-5',M3}(x) + k_{1',M3}(x) + k_{-w2}(x) + k_{w3}(x)) \cdot A'M_3(x, t) - v(\delta A'M_3(x, t)/\delta x)$;

$\delta\ A'M_4(x, t)/\delta t = k_{5',M4}(x)\ A'M_4ADP(x, t) + k_{-1',M4}(x)MATP(x, t) + k_{w3}(x)\ A'M_3(x, t) - (k_{-5',M4}(x) + k_{1',M4}(x) + k_{-w3}(x)) \cdot A'M_4(x, t) - v(\delta A'M_4(x, t)/\delta x)$;

References

Barclay CJ, Woledge RC & Curtin NA. (2010). Inferring crossbridge properties from skeletal muscle energetics. *Prog Biophys Mol Biol* **102,** 53-71.

Brenner B & Yu LC. (1991). Characterization of radial force and radial stiffness in Ca(2+)-activated skinned fibres of the rabbit psoas muscle. *J Physiol* **441,** 703-718.

Brunello E, Reconditi M, Elangovan R, Linari M, Sun YB, Narayanan T, Panine P, Piazzesi G, Irving M & Lombardi V. (2007). Skeletal muscle resists stretch by rapid binding of the second motor domain of myosin to actin. *Proc Natl Acad Sci U S A* **104,** 20114-20119.

Caremani M, Dantzig J, Goldman YE, Lombardi V & Linari M. (2008). Effect of inorganic phosphate on the force and number of myosin cross-bridges during the isometric contraction of permeabilized muscle fibers from rabbit psoas. *Biophys J* **95,** 5798-5808.

Huxley AF & Simmons RM. (1971). Proposed mechanism of force generation in striated muscle. *Nature* **233,** 533-538.

Kawai M, Wray JS & Zhao Y. (1993). The effect of lattice spacing change on cross-bridge kinetics in chemically skinned rabbit psoas muscle fibers. I. Proportionality between the lattice spacing and the fiber width. *Biophys J* **64,** 187-196.

Linari M, Caremani M & Lombardi V. (2010). A kinetic model that explains the effect of inorganic phosphate on the mechanics and energetics of isometric contraction of fast skeletal muscle. *Proc Biol Sci* **277,** 19-27.

Linari M, Caremani M, Piperio C, Brandt P & Lombardi V. (2007). Stiffness and fraction of Myosin motors responsible for active force in permeabilized muscle fibers from rabbit psoas. *Biophys J* **92,** 2476-2490.

Park-Holohan S, Linari M, Reconditi M, Fusi L, Brunello E, Irving M, Dolfi M, Lombardi V, West TG, Curtin NA, Woledge RC & Piazzesi G. (2012). Mechanics of myosin function in white muscle fibres of the dogfish, Scyliorhinus canicula. *J Physiol* **590,** 1973-1988.

Piazzesi G & Lombardi V. (1995). A cross-bridge model that is able to explain mechanical and energetic properties of shortening muscle. *Biophys J* **68,** 1966-1979.

Piazzesi G, Lucii L & Lombardi V. (2002). The size and the speed of the working stroke of muscle myosin and its dependence on the force. *J Physiol* **545,** 145-151.

Rayment I, Rypniewski WR, Schmidt-Base K, Smith R, Tomchick DR, Benning MM, Winkelmann DA, Wesenberg G & Holden HM. (1993). Three-dimensional structure of myosin subfragment-1: a molecular motor. *Science* **261,** 50-58.

Woledge RC, Barclay CJ & Curtin NA. (2009). Temperature change as a probe of muscle crossbridge kinetics: a review and discussion. *Proc Biol Sci* **276,** 2685-2695.